

# Study of N 2 as a Mean to Improve CO 2 Storage Safety

Dan Bossie-Codreanu

▶ **To cite this version:**

Dan Bossie-Codreanu. Study of N 2 as a Mean to Improve CO 2 Storage Safety. Energy Procedia, 2017, 114, pp.5479 - 5499. 10.1016/j.egypro.2017.03.1691 . hal-01739953

**HAL Id: hal-01739953**
**https://ifp.hal.science/hal-01739953**

Submitted on 21 Mar 2018

**HAL** is a multi-disciplinary open access archive for the deposit and dissemination of scientific research documents, whether they are published or not. The documents may come from teaching and research institutions in France or abroad, or from public or private research centers.

L'archive ouverte pluridisciplinaire **HAL**, est destinée au dépôt et à la diffusion de documents scientifiques de niveau recherche, publiés ou non, émanant des établissements d'enseignement et de recherche français ou étrangers, des laboratoires publics ou privés.



Distributed under a Creative Commons Attribution - NonCommercial - NoDerivatives| 4.0 International License

Available online at www.sciencedirect.com

ScienceDirect

Energy Procedia 114 (2017) 5479 – 5499

Energy Procedia

13th International Conference on Greenhouse Gas Control Technologies, GHGT-13, 14-18 November 2016, Lausanne, Switzerland

# Study of $N_2$ as a Mean to Improve $CO_2$ Storage Safety

Dan Bossie-Codreanu

*IFPEN, 1 et 4 Av. Bois-Préau, 92852 Rueil-Malmaison, France*

**Abstract**

Current $CO_2$ storage operations in aquifer reservoirs are naturally limited, among other parameters, by entry pressures encountered in cap-rocks, thus limiting over-pressures allowed during the storage process. The injection of nitrogen in a zone just below the cap-rock, prior $CO_2$ injection, could be a viable protective measure to increase the storage safety by lowering the leakage risk and increasing the maximum allowable reservoir pressure.

The physical background of the beneficial impact of Nitrogen on the caprock entry pressure is based on the higher $N_2$–brine interfacial tension (IFT) compared to $CO_2$–brine. As a maximum possible effect (for pure $N_2$-brine systems), IFT could increase by a factor of two, yielding correspondingly to the same increase of allowable pressure. However, the $N_2$ injection decreases the storage volume and the trade-off must be studied carefully. The IFT spread decreases rapidly with the mixing ratio of $CO_2$ in the $N_2$. Mixing can occur due to advective processed induced by differential absolute pressure due to $CO_2$ injection and also due to vertical mixing due to different partial pressure. Injection placement is carefully studied carefully, especially the vertical conformance as well as saturation rarefaction.

In order to study the feasibility of such approach for different storage conditions, a series of $CO_2$ injection simulations were performed within a generic characterization framework based on dimensionless numbers. A database of dimensionless numbers governing the storage was build, using literature information. The application of an experimental design based on the minimum/maximum values found within the data-base identified a series of cases to be simulated, further reduced by a fractional approach of such design. The scenarios simulated consisted in a $CO_2$ injection within a reservoir storage zone found at some distance from the $N_2$ zone, just below the cap-rock, followed by a resting period during which the $CO_2$ saturation is monitored. The $N_2$ zone is refined, rendering possible the study of the the potential mixing and contamination with $CO_2$. For all case members of the data base, the $CO_2$ conformance was studied in terms of possible mixing and override of the $CO_2$ plume. Discussion of the potential benefits and possible difficulties are addressed. Conclusions were drawn considering the possible field application of such a technique, identifying a-priori sites more suitable for such a technique, based on the dimensionless numbers characterizing them.

© 2017 The Authors. Published by Elsevier Ltd. This is an open access article under the CC BY-NC-ND license (http://creativecommons.org/licenses/by-nc-nd/4.0/).
Peer-review under responsibility of the organizing committee of GHGT-13.

1876-6102 © 2017 The Authors. Published by Elsevier Ltd. This is an open access article under the CC BY-NC-ND license (http://creativecommons.org/licenses/by-nc-nd/4.0/).
Peer-review under responsibility of the organizing committee of GHGT-13.
doi:10.1016/j.egypro.2017.03.1691

*Keywords:* $CO_2$ Storage;$N_2$ Injection;Mixing;Methodology

## 1. Introduction

Storage of $CO_2$ currently is naturally limited by entry-pressure values of the cap-rock, which is a limiting factor in terms of storage capacity. One method which has been suggested as being effective in protecting the cap-rock is the injection of $N_2$, which is supposed to act not only in shielding the cap-rock from the $CO_2$ but also increasing the IFT which controls the $CO_2$ entry.

The concept governing the injection of $N_2$ is summarized below.

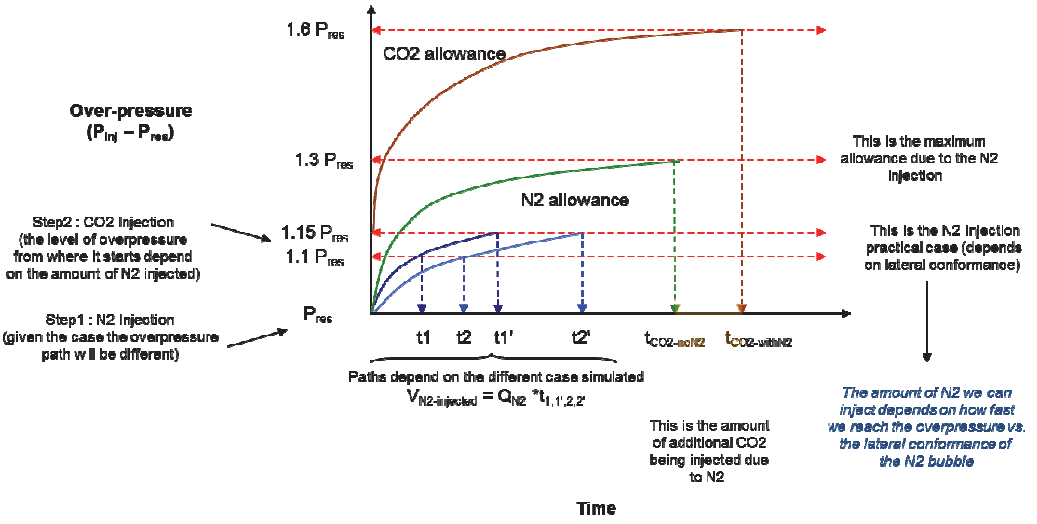



Figure 1. Conceptual design of an N2 injection prior to a $CO_2$ injection

The conceptual schematic showing the $N_2$ injection (Figure 1) considers a first injection step made up only of the $N_2$, followed by the injection of the $CO_2$. Within this scheme, the allowable overpressure for the $N_2$ needs to be set with regard to the cap-rock, which subsequently defines how much $CO_2$ can be injected in a second step. This implies a double design; one concerning the injection of the $N_2$, followed by the $CO_2$, within a framework in which the overall overpressure allowance is studied and decided for the storage, considering both gases instead of only one (the $CO_2$). Furthermore, the areal conformance of the $N_2$ within the injection layer should be considered since the protective nature of the $N_2$ should cover the entire $CO_2$ plume extension.

Considerations above concern a possible injection of $N_2$ as a mean to increase capacity while protecting the storage site against leaking risks. The process of the $N_2$ injection envisioned as a cushion gas as well as possibly enhancing storage capacities has been patented by IFPEN (Barroux, [24] ). Several authors have recently shown interest in the co-injection of $CO_2$ and $N_2$ (Fisher *et al*. [25] and Wei et al. [26]). Yet, their interest concerned more the $N_2$ as a tracer rather than a gas to be used as a cushion gas. From the thermodynamic point of view the IFT properties are a-priori favorable for the design of such a process.

Yet, issues have been raised about the possible mixing between the $CO_2$ and the $N_2$ occurring below the cap-rock, where in principle the $N_2$ needs to be placed, thus lessening the potential protection caused by this gas cushion.

Before discussing more critical issues such as the effective volumes needed to provide a thorough conformance of the $N_2$ below the cap-rock, or the study of the overall overpressure allowance, the present study investigates the possibility of mixing between the two gases. The $N_2$ is supposed to have been injected in a layer below the cap-rock. Several $CO_2$ injection scenarios within a reservoir storage zone are, below the protecting $N_2$ zone, followed by a resting period, are simulated, investigating the $CO_2$ movement within the full field (during the injection, after the injection and finally at the end of a 10 year period of rest – the resting period was chosen ad-hoc). For that a dimensionless approach, consisting in generating numbers governing the $CO_2$ injection were generated, studying the gas saturation corresponding to a typical $CO_2$ injection, followed by a resting period during which the movement of the $CO_2$ is recorded, along with the overpressure. The goal of the study is to determine which dimensionless numbers govern favorable conditions for the $CO_2$ confinement within the storage zone, including the resting period.

The $CO_2$ saturation is analyzed using the dimensionless numbers supposed to characterize the different reservoirs, drawing conclusions about the mixing characteristics below the cap-rock in regard to the dimensionless numbers characterizing the storage setting.

## 2. Building the Problem

### *2.1. Theoretical Foundations*

The movement of $CO_2$ in the groundwater aquifer during injection, potential leaking and possible remediation is complex and depends on the interplay of many factors. These factors include gravity effects, capillary forces, and viscous forces as well as the impacts from dissolution/ex-solution of the $CO_2$ with the water. In order to obtain a "generic" simulation framework, the following methodology followed was applied:

Step1: Dimensionless Numbers and Experimental Design Definition

- Definition of process dimensionless Numbers (DN). A series of pertinent dimensionless numbers governing injection and evolution of the $CO_2$ plume, using pertinent knowledge obtained by the oil industry (reservoir engineering).
- Building a data base (DB) of DN. Based on parameters making up the dimensionless numbers, an investigation of their value was collected from field cases already performed, using literature data, and a DB build accordingly.
- Using the value range of each DN, a Min/Max criteria allowed a fractional experimental design, thus reducing the number of cases.

Step2: Definition of a series of scenarios of $CO_2$ production. Based on the above a series of simulation covering all possible cases was build and several production scenarios were considered, stemming from a common initial $CO_2$ injection scheme which establishes an average original saturation field. These scenarios account for the rate production, acknowledging the possibility of water coning, which in the case of $CO_2$ production can be favorable, since it will favor the production of water which is probably easier to dispose.

Step3: Perform simulations on all cases defined in Step2

Step4: Analyze results and define criteria by which simulations will be evaluated in terms of safety and process performance (ex. % of $CO_2$ recovered by comparison to $CO_2$ injected).

Theoretically, the dimensionless numbers which can used have been identified using literature of $CO_2$-EOR which aimed originally at scaling the $CO_2$ injection Shook *et al*. [1], Rivas *et al*. [2], Diaz *et al.* [3]. Scaling consists in extrapolating results obtained at one scale size to another scale. This process produces dimensionless groups, which then serve as a basis of comparison between scales. These are combination of properties such that the dimensions of the properties composing the dimensionless group cancel each other to produce a final group with no dimensions. A process can be described by independent and dependent dimensionless variables. When the independent dimensionless groups for that group are identical, the dependent dimensionless group will also be identical. This implies that systems with completely different dimensional properties but similar dimensionless properties have a similar dimensionless response, allowing a comparison between scales. The dimensionless groups retained for the description of the injection/production $CO_2$ process are:

Aspect Ratio ($R_L$): This is a measure of the communication between fluids in the horizontal direction relative to the vertical one. The aspect ratio governs the vertical equilibrium (VE), representing the state of maximum cross-flow, occurring when the forces in the transverse direction is zero. The greater the aspect ratio, the closer it is to vertical equilibrium (well approximated for aspect ratios greater than 10).

$$R_L = \frac{L}{H}\sqrt{\frac{k_z}{k_x}} \tag{1}$$

where L is the reservoir length, H is the thickness, $k_z$ is the vertical permeability and $k_x$ is the horizontal permeability.

Dip angle group (Nα): Long, thin, dipping reservoirs will have greater values of Nα, lessening the potential impact of gravity overriding, while thicker, shorter reservoirs (low Nα) increase the potential impact of gravity overriding.

$$N_\alpha = \frac{L}{H}\tan\alpha \tag{2}$$

where α is the reservoir angle with the horizontal

Mobility Ratio (M): Mobility relates the ability of gas and water to move relative to each other and are used to evaluate sweep efficiencies.

$$M_g^w = \frac{k_{rg}^o \mu_w}{k_{rw}^o \mu_g} \tag{3}$$

where $\mu_g$ and $\mu_w$ are gas and water viscosity and $Kr_g^\circ$ and $Kr_w^\circ$ are relative permeability end-points for gas and water

Buoyancy Number (Ng): The buoyancy number is the ratio of the gravity forces resulting of the density difference to the viscous forces in a reservoir. Larger values of Ng indicate larger density differences between fluids and therefore a higher potential for segregation. Thus, the Ng value governs the shape of the $CO_2$ from its injection point (lower Ng values favoring a more cylindrical shape).

$$N_g = \frac{H\Delta\rho g\cos\alpha}{\Delta P} \tag{4}$$

where Δρ is the density between gas sand water, g is the gravity constant and ΔP is the difference in pressure between the injection and the reservoir.

Capillary Number (NPc): The capillary number is the ratio of the viscous forces to the capillary ones. It governs the amount of trapping which may occur in an aquifer storage. Capillary forces increase with capillary pressure.

$$N_{Pc} = \frac{\Delta P}{\sigma}\sqrt{\frac{k}{\phi}} \tag{5}$$

where σ is the interfacial tension and φ is the porosity.

Heterogeneity (VDP) – Dykstra-Parsons method: This method is simple, allowing the generation of a vertical (and possibly horizontal) permeability heterogeneity. It is expressed as a variance of the permeability where $K_x$ is the permeability with a probability of x %. The index is expressed by:

$$VDP = \frac{K_{50} - K_{84.1}}{K_{50}} \tag{6}$$

The significance of such a definition can be seen in Figure 2.

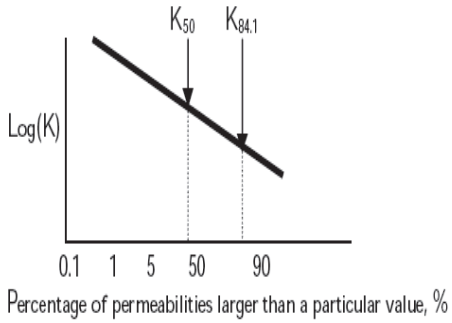



Figure 2. Illustration of the VDP concept

A completely homogeneous system has a VDP = 0 and a completely heterogeneous system has a VDP = 1. Heterogeneity is viewed as a layered system to which a permeability is assigned per layer. Thus, the method used in this study consists in assuming some VDP value (from statistics issued from hydrocarbon reservoirs), and then assign a permeability to each layer, inverting the VDP function. Vertical permeability is calculated from the horizontal value (ex. $K_z = 0.1\ K_x$). Porosity is assigned from the K-PHI relationship corresponding to the field under study, often available.

The question may be raised on why geostatistical methods are not used here. The answer is simple. Geostatistical data such as correlation lengths obtained from variogram analysis imply the existence of many wells so as to determine the existence of such correlations lengths. Furthermore, if correlative relations could be found at the facies "level", such as porosity which can be correlated for particular deposition environments it is hardy the case for permeability (outcrop studies have proven that). Using petrophysical properties for characterization would need the development of flow-units, which is not easy to Data base of geostatistical parameters for aquifers or hydrocarbon reservoirs are not easy to come by. By opposition, VDP statistics for many reservoirs have been collected (Hirasaki *et al* [4], Jensen *et al.* [5], Dykstra *et al.* [6]) and thus we can use these for our modeling purpose. While recognized as being imperfect, this method accounting for heterogeneity, given its simplicity, is considered as adequate for this study.

In our case, two representative values of VDP were considered - VDP = 0.6 and 0.8 as seen in Figure 3 below (Hirasaki *et al* [5].

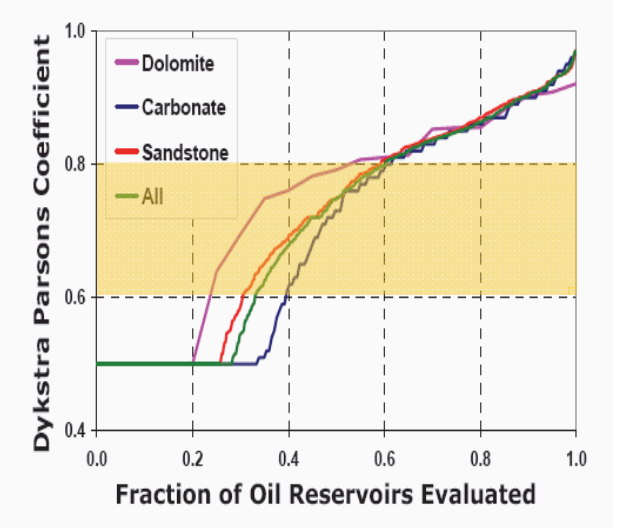



Figure 3. VDP value depending on the reservoir type

Injection pressure ($P_i$): This ratio determines the dimensionless injection pressure with regard to the fracturing pressure, considered as a limiting pressure for CO2 operations. For all simulations cases two scenarios were chosen, based on over-pressure data obtained from traditional CH4 storage operations.

$$P_i = \frac{P_{inj}}{P_{fract}} \tag{7}$$

Residual gas saturation ($S_{gr}$): Residual gas saturation controls the volume of gas trapped in that portion of the reservoir that has experienced water encroachment. As water moves into a rock volume filled with gas, the water displacement of the gas is incomplete. The water fills pores and pore throats, causing capillary pressure and relative permeability effects to stop the flow of gas and allow only water to pass through the rock volume. This results in gas being trapped behind the encroaching waterfront as residual gas. The volume and location of the residual gas are controlled by the distribution of the petrophysical properties. The trapping characteristics used were calculated from the relation of Holtz [22].

### *2.2 Data Base Building*

The data-base of dimensionless numbers was built from information obtained from different publications describing field injections (Bachu *et al*. [7]., Bachu S. [8], Flett *et al*. [9], Hosa *et al*. [10] ). The total number of sites qualifying for the data base is 60, of which 40 are aquifers and 20 reservoirs.

The theoretical analysis identified eight dimensionless groups characterizing the $CO_2$ storage. Further analysis of the available data lead to a reduction of the groups considered. Thus, only five groups were retained to represent the variability of all cases, namely the Aspect Ratio ($R_L$), the Dip angle group ($N_\alpha$), the Mobility Ratio (M), the Buoyancy Number ($N_g$) and the Capillary Number ($N_{Pc}$). The other groups, namely the Residual gas saturation, VDP

and Injection Pressure are estimated, making up the different simulation group scenarios. Results from the Data-Base are shown below in Figure 4 through 9.

Aspect ratio

Min = 1.58

Max = 6.32

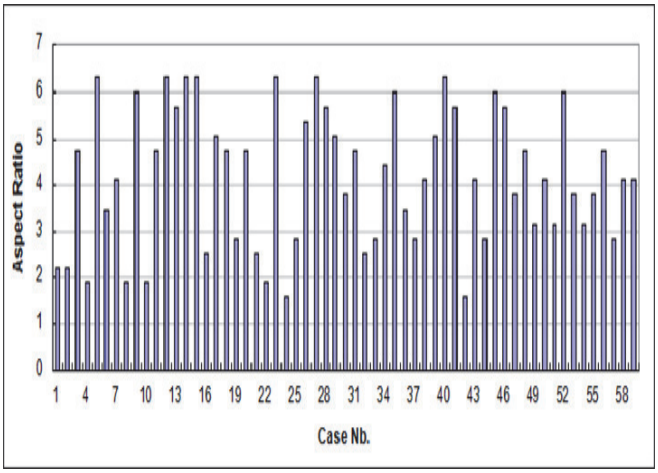



Figure 4. Aspect Ratio obtained for all investigated cases

As seen, no value among all cases considered reaches a value of 10, which is theoretically a value approximating a perfect vertical equilibrium.

Dip Number

Min = 0.17

Max = 3.52

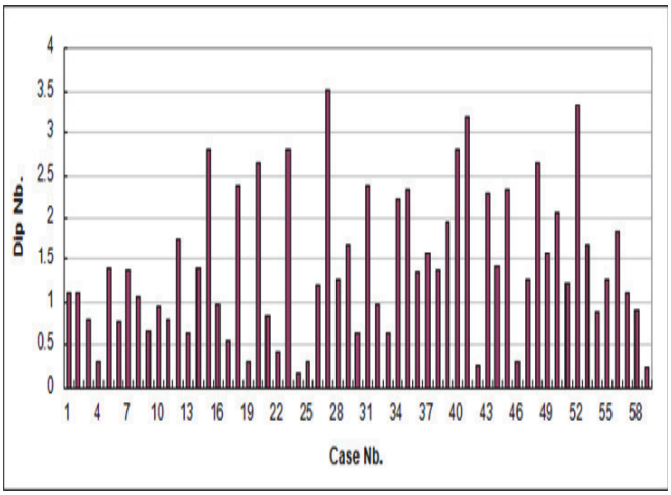



Figure 5. Aspect Ratio distribution obtained for all investigated cases

Long, thin dipping reservoirs have greater Dip Angle numbers, lessening the potential impact of gravity overriding. It also has an impact on the shape of the interface between displaced and displacing fluids. The lower the value of the number the more the interface parallel to the fluid movement. By opposition, the higher the value,

the is most perpendicular to the fluid movement. In developing the statistic angle values varying between 1 and 10 degrees were used.

Mobility Ratio

Min = 1.44

Max = 54.06

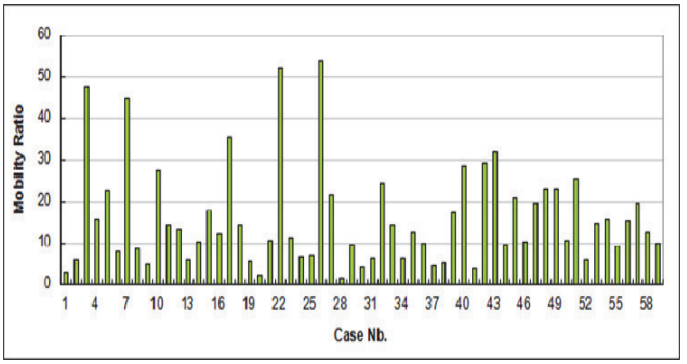


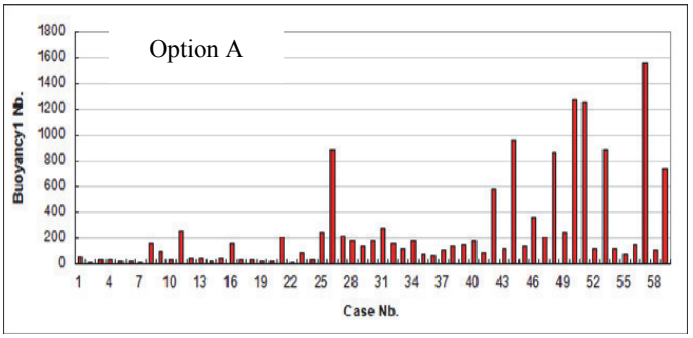

Figure 6. Mobility Ratio distribution obtained for all investigated cases

This is the ratio of the viscous forces of one fluid relative to the other. In theory the closest the ratio is to 1.0 the more stable the recovery of $CO_2$ will be. High values such as the ones recorded here using our data base of aquifer projects shows values up to 54.0 (for oil reservoirs it can go up to 45.0), indicative of conditions where displacement will be highly unfavorable.

Buoyancy Number

Min = 13.89

Max = 1562.1




Min = 1.73

Max = 195.26

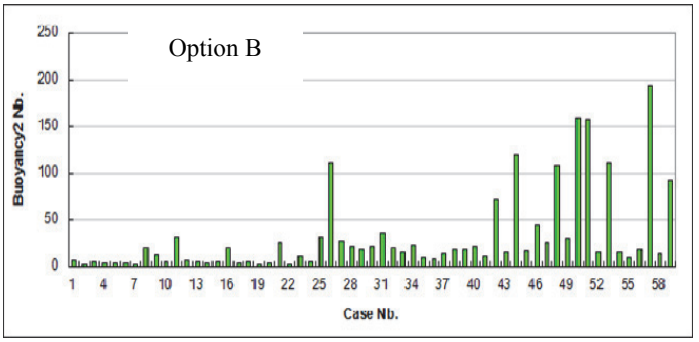


Figure 7. Buoyancy Number distribution obtained for all investigated cases (Option A -Top and B - Bottom)

The buoyancy group requires a ΔP term between the injection pressure and the reservoir pressure. The injection pressure is related to the fracturing pressure which represents a potential risk when storing the $CO_2$ - the risk not being necessarily the fracture itself, but the potential impact it could create on the well completion (cementation), thus creating a potential leaking path. Thus, two hypothesis are made. The first one assumes that $P_{inj} = 1.1P_{res}$ (option a) while the second one is that $P_{inj} = 1.8P_{res}$ (option b). Results are shown below. Given the fact that the only values changing between the two options are the injection pressure, the variability among values stays the same.

Capillary Number

The capillary group variability is shown below (Figure 8).

Min = 1.4E-04

Max = 3E-03

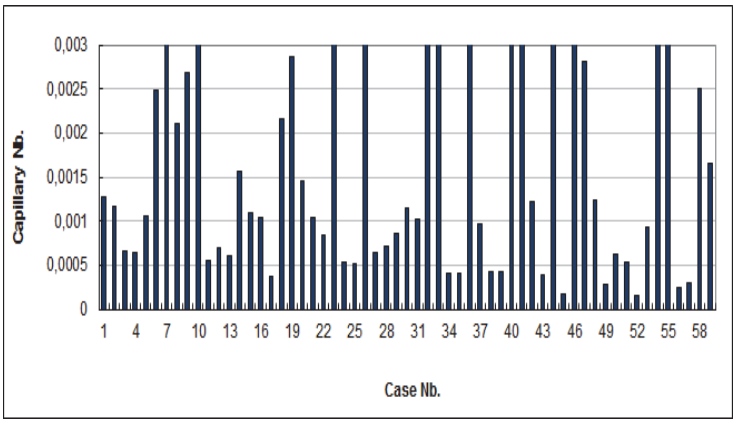



Figure 8. Capillary Number distribution obtained for all investigated cases

Like the other constitutive relationships describing multiphase flow, capillary pressure and relative permeability, the IR characteristic of a rock is considered to be invariant across a wide range of fluid pairs and conditions of temperature, pressure and brine salinity so long as the wetting state of the system remains similar between systems.

It is well known that these properties will vary, however, and if these conditions control the wetting state of the system (Salathiel [11]) or the flow velocity v, viscosity μ and interfacial tension σ combine in a way such that the dimensionless capillary number, $Nc = v\mu/\sigma$, exceeds a critical value for desaturation. For Berea sandstone, for example, this has been observed to be in the range $Nc > 10^{-5}$ - $10^{-4}$ (Taber [12]). For natural rocks representative of a wide variety of pore structures the range of capillary numbers for desaturation extends to $Nc > 10^{-7} - 10^{-4}$ (Lake et al., [13]). Observations of the wetting state of the CO2 brine system have raised doubts about whether these general observations extend to CO2 displacement. Contact angle, conventionally measured in the wetting phase, water, was observed to increase (weakening water wetting) with pressure in work of Broseta *et al*. [14] Chiquet *et al*. [15] or Iglauer *et al.* [16] , by opposition to the work of Espinoza *et al.* [17], Farokhpoor *et al.* [18], and Wang et al. [19]. Contact angle was observed to increase significantly with brine salinity in work by Espinoza et al. [17],, but not in Broseta *et al.* [14], Chiquet *et al.* [15]. The work of Farokhpoor *et al.* [18], Saraji *et al.* [20] investigated the dependency of contact angle on temperature but a clear trend was not observed. A recent review of the subject (Iglauer *et al* [21].) highlights the challenging nature of these experiments and summarizes that the wide range of behavior observed can be attributed largely to differences in surface roughness and surface contamination between studies. Thus, it is difficult a-priori to estimate the role this number will play during the simulation of an injection/production process as envisioned here. We expect the residual saturation to play a larger role through the Kr trapping effects and thus indirectly reflecting the importance of capillary trapping.

The Sgr term

In addition to all the dimensionless groups chosen as representative of the CO2 storage, the maximum gas strapping saturations are shown, in order to define a representative value range to be used with all scenarios (see Figure 9).

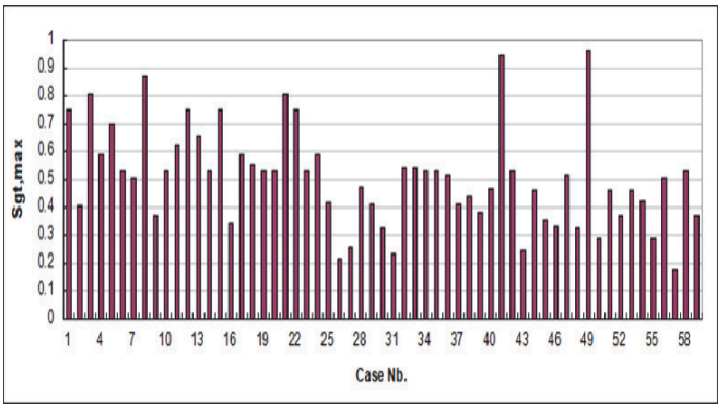



Figure 9. $Sgt_{max}$ distribution obtained for all investigated cases

When studying the distribution of reservoirs within our data-base by $Sgt_{max}$ class-values, we observe very high values of trapped gas saturations for reservoirs of low porosity values. These potential candidates should be excluded from potential storage sites given their porosity values which in term controls the storage capacity.

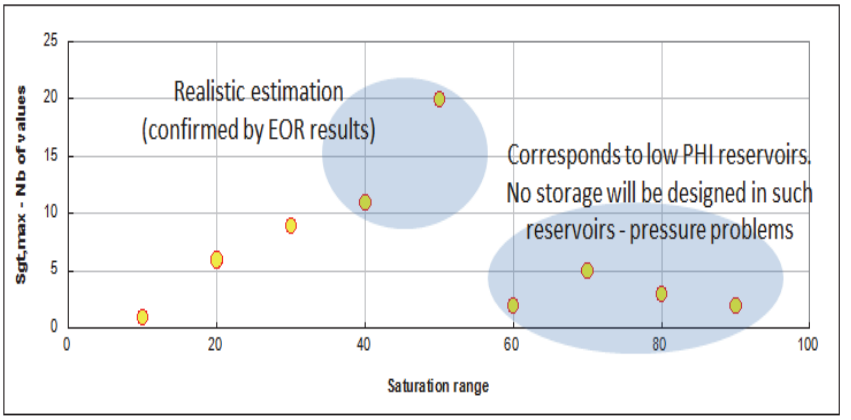



Figure 10. Reservoir distribution classified by trapped gas saturation values

The value most representative are considered as $S_{gtmax}$ = 0.45. The EOR operations have shown from a simple material balance (amount of $CO_2$ injected – amount of $CO_2$ produced) that about 40 to 50 % of the $CO_2$ injected stays trapped. These numerical figures are worth considering over eventual core-floods since they are obtained at a macroscopic scale (realistic scale), as seen in Figure 10.

From all the dimensionless terms defined above, considering a representative variability we are looking after, and considering the min/max values of all dimensionless groups, we designed 4 main scenarios, shown below in Figure 11.

| Scenario 1 | -1 | 1 |
|---|---|---|
| VDP | 0.6 | |
| | Min | Max |
| Aspect Ratio | 1.58 | 6.32 |
| Dip | 0.17 | 3.52 |
| Mobility Ratio | 1.44 | 54.06 |
| Buoyancy1 | 13.89 | 1562.1 |
| Capillary | 0.000301 | 4.68 |

| Scenario 2 | -1 | 1 |
|---|---|---|
| VDP | 0.6 | |
| | Min | Max |
| Aspect Ratio | 1.58 | 6.32 |
| Dip | 0.17 | 3.52 |
| Mobility Ratio | 1.44 | 54.06 |
| Buoyancy1 | 1.73 | 195.26 |
| Capillary | 0.000301 | 4.68 |

| Scenario 3 | -1 | 1 |
|---|---|---|
| VDP | 0.8 | |
| | Min | Max |
| Aspect Ratio | 1.58 | 6.32 |
| Dip | 0.17 | 3.52 |
| Mobility Ratio | 1.44 | 54.06 |
| Buoyancy1 | 13.89 | 1562.1 |
| Capillary | 0.000301 | 4.68 |

| Scenario 4 | -1 | 1 |
|---|---|---|
| VDP | 0.8 | |
| | Min | Max |
| Aspect Ratio | 1.58 | 6.32 |
| Dip | 0.17 | 3.52 |
| Mobility Ratio | 1.44 | 54.06 |
| Buoyancy1 | 1.73 | 195.26 |
| Capillary | 0.000301 | 4.68 |

Figure 11. All scenarios considering values of dimensionless numbers

The Scenarios above consider two VDP values (0.6 and 0.8), along with two buoyancy numbers (corresponding to two injection conditions; one leading to higher overpressures after 4 years than the other – these numbers being derived from a pressure difference formulation between reservoir pressure and injection pressure.

In summary six numbers are considered (including two different buoyancy numbers) but only five are considered for an experiment design for each VDP chosen (in our case 0.6 and 0.8)

*2.3 Experimental Design & Optimization*

The design of experiments (in our case simulations) is a planned approach aiming to determine cause and effect relationships, applied to any process with measurable inputs and outputs. The aim of designing experiments is to identify the factors which cause changes in the responses, and predicting them in a simple mathematical form. In our case we used a fractional factorial design to reduce the number of simulations to be run in order to obtain a representative response relationship.

Factorial design means that all possible combinations of the levels of the factors are investigated in each complete trial or replication of the experiment (simulation). One of the most widely used case of factorial design is using K factors with two levels. These two levels are denoted as (-1) for the minimum value and (+1) for the maximum one. Therefore, a $2^k$ factorial design requires $2^k$ runs to perform the analysis. For a five dimensionless group problem, considering the maximum and minimum values, the total number of simulations to perform are 32. In our case since four main scenarios are considered, 128 simulation in theory cover the entire “experiment”, including all interactions. This is shown in Figure 11 in which A= Aspect Ratio, B=Dip Number, C= Mobility Ratio, D= Buoyancy Number (either 1 or 2 depending on the injection scheme chosen) and E= Capillary Number.

Results of the full experimental design are shown in Figure 12, including the interaction terms, considering all parameters (5 parameters) or any combination (2,3 or 4 parameters) . Along with the full experimental design, the sum of all parameters is shown in the last column, helping in reducing the number of simulations.

| | A | B | C | D | E | ABCDE | AB | AC | AD | AE | BC | BD | BE | CD | CE | DE | ABC | ACD | ADE | BCD | BDE | CDE | ABCD | BCDE | Sum |
|---|---|---|---|---|---|---|---|---|---|---|---|---|---|---|---|---|---|---|---|---|---|---|---|---|---|
| 1 | 1 | 1 | 1 | 1 | 1 | 1 | 1 | 1 | 1 | 1 | 1 | 1 | 1 | 1 | 1 | 1 | 1 | 1 | 1 | 1 | 1 | 1 | 1 | 1 | 10 |
| 2 | -1 | 1 | 1 | 1 | 1 | -1 | -1 | -1 | -1 | -1 | 1 | 1 | 1 | 1 | 1 | 1 | -1 | -1 | -1 | 1 | 1 | 1 | -1 | 1 | 2 |
| 3 | 1 | -1 | 1 | 1 | 1 | -1 | -1 | 1 | 1 | 1 | -1 | -1 | -1 | 1 | 1 | 1 | -1 | 1 | 1 | -1 | -1 | 1 | -1 | -1 | 0 |
| 4 | 1 | 1 | -1 | 1 | 1 | -1 | 1 | -1 | 1 | 1 | -1 | 1 | 1 | -1 | -1 | 1 | -1 | -1 | 1 | -1 | 1 | -1 | -1 | -1 | -2 |
| 5 | 1 | 1 | 1 | -1 | 1 | -1 | 1 | 1 | -1 | 1 | 1 | -1 | 1 | -1 | 1 | -1 | 1 | -1 | -1 | -1 | -1 | -1 | -1 | -1 | -4 |
| 6 | 1 | 1 | 1 | 1 | -1 | -1 | 1 | 1 | 1 | -1 | 1 | 1 | -1 | 1 | -1 | -1 | 1 | 1 | -1 | 1 | -1 | -1 | 1 | -1 | 2 |
| 7 | -1 | -1 | 1 | 1 | 1 | 1 | 1 | -1 | -1 | -1 | -1 | -1 | -1 | 1 | 1 | 1 | -1 | -1 | -1 | -1 | -1 | 1 | 1 | -1 | -4 |
| 8 | 1 | -1 | -1 | 1 | 1 | 1 | -1 | -1 | 1 | 1 | 1 | -1 | -1 | -1 | -1 | 1 | 1 | -1 | 1 | 1 | -1 | -1 | 1 | 1 | 0 |
| 9 | 1 | 1 | -1 | -1 | 1 | 1 | 1 | -1 | -1 | 1 | -1 | -1 | 1 | 1 | -1 | -1 | -1 | 1 | -1 | 1 | -1 | 1 | 1 | 1 | 0 |
| 10 | 1 | 1 | 1 | -1 | -1 | 1 | 1 | 1 | -1 | -1 | -1 | -1 | -1 | -1 | 1 | 1 | -1 | 1 | 1 | -1 | 1 | 1 | -1 | 1 | 0 |
| 11 | -1 | -1 | -1 | 1 | 1 | -1 | 1 | 1 | -1 | -1 | 1 | -1 | -1 | -1 | -1 | 1 | -1 | 1 | -1 | 1 | -1 | -1 | -1 | 1 | -4 |
| 12 | 1 | -1 | -1 | -1 | 1 | -1 | -1 | -1 | -1 | 1 | 1 | 1 | -1 | 1 | -1 | -1 | 1 | 1 | -1 | -1 | 1 | 1 | -1 | -1 | -2 |
| 13 | 1 | 1 | -1 | -1 | -1 | -1 | 1 | -1 | -1 | -1 | 1 | 1 | 1 | -1 | 1 | 1 | -1 | 1 | 1 | 1 | -1 | 1 | -1 | -1 | 0 |
| 14 | -1 | -1 | -1 | -1 | 1 | 1 | 1 | 1 | 1 | -1 | 1 | 1 | -1 | 1 | -1 | -1 | -1 | -1 | 1 | -1 | 1 | 1 | 1 | -1 | 2 |
| 15 | 1 | -1 | -1 | -1 | -1 | 1 | -1 | -1 | -1 | -1 | 1 | 1 | 1 | 1 | 1 | 1 | 1 | 1 | 1 | -1 | -1 | -1 | -1 | 1 | 2 |
| 16 | -1 | -1 | -1 | -1 | -1 | -1 | 1 | 1 | 1 | 1 | 1 | 1 | 1 | 1 | 1 | -1 | -1 | -1 | -1 | -1 | -1 | -1 | 1 | 1 | 6 |
| 17 | 1 | -1 | -1 | -1 | -1 | 1 | -1 | -1 | -1 | -1 | 1 | 1 | 1 | 1 | 1 | 1 | 1 | 1 | 1 | -1 | -1 | -1 | -1 | 1 | 2 |
| 18 | -1 | 1 | -1 | -1 | -1 | 1 | -1 | 1 | 1 | 1 | -1 | -1 | -1 | 1 | 1 | 1 | 1 | -1 | -1 | 1 | 1 | -1 | -1 | -1 | 0 |
| 19 | -1 | -1 | 1 | -1 | -1 | 1 | 1 | -1 | 1 | 1 | -1 | 1 | 1 | -1 | -1 | 1 | 1 | -1 | -1 | 1 | -1 | 1 | -1 | -1 | 2 |
| 20 | -1 | -1 | -1 | 1 | -1 | 1 | 1 | 1 | -1 | 1 | -1 | 1 | -1 | 1 | -1 | -1 | -1 | 1 | 1 | 1 | 1 | 1 | -1 | -1 | 4 |
| 21 | -1 | -1 | -1 | -1 | 1 | 1 | 1 | 1 | 1 | -1 | 1 | 1 | -1 | 1 | -1 | -1 | -1 | -1 | 1 | -1 | 1 | 1 | 1 | -1 | 2 |
| 22 | 1 | 1 | -1 | -1 | -1 | -1 | 1 | -1 | -1 | -1 | -1 | 1 | 1 | 1 | 1 | -1 | 1 | 1 | 1 | 1 | 1 | -1 | 1 | -1 | 0 |
| 23 | -1 | 1 | 1 | -1 | -1 | -1 | -1 | -1 | 1 | 1 | 1 | -1 | -1 | -1 | -1 | 1 | -1 | 1 | -1 | -1 | 1 | 1 | 1 | 1 | 0 |
| 24 | -1 | -1 | 1 | 1 | -1 | -1 | 1 | -1 | -1 | 1 | -1 | -1 | 1 | 1 | -1 | -1 | 1 | -1 | 1 | -1 | 1 | -1 | 1 | 1 | 0 |
| 25 | -1 | -1 | -1 | 1 | 1 | -1 | 1 | 1 | -1 | -1 | 1 | -1 | -1 | -1 | 1 | 1 | -1 | 1 | -1 | 1 | -1 | -1 | -1 | 1 | -4 |
| 26 | 1 | 1 | 1 | -1 | -1 | 1 | 1 | 1 | -1 | -1 | 1 | -1 | -1 | -1 | -1 | 1 | 1 | -1 | 1 | -1 | 1 | 1 | -1 | 1 | 0 |
| 27 | -1 | 1 | 1 | 1 | -1 | 1 | -1 | -1 | -1 | 1 | 1 | 1 | -1 | 1 | -1 | -1 | -1 | -1 | 1 | 1 | -1 | -1 | -1 | -1 | -6 |
| 28 | -1 | -1 | 1 | 1 | 1 | 1 | 1 | -1 | -1 | -1 | -1 | -1 | 1 | 1 | 1 | 1 | -1 | -1 | -1 | -1 | 1 | 1 | 1 | -1 | -4 |
| 29 | 1 | 1 | 1 | 1 | -1 | -1 | 1 | 1 | 1 | -1 | 1 | 1 | -1 | 1 | -1 | -1 | 1 | 1 | -1 | 1 | -1 | -1 | 1 | -1 | 2 |
| 30 | -1 | 1 | 1 | 1 | 1 | -1 | -1 | -1 | -1 | -1 | 1 | 1 | 1 | 1 | 1 | 1 | -1 | -1 | -1 | 1 | 1 | 1 | -1 | 1 | 2 |
| 31 | 1 | -1 | 1 | -1 | 1 | 1 | -1 | 1 | -1 | 1 | -1 | 1 | -1 | -1 | 1 | -1 | -1 | 1 | 1 | -1 | 1 | 1 | 1 | -1 | -2 |
| 32 | -1 | 1 | -1 | 1 | -1 | -1 | -1 | 1 | -1 | 1 | -1 | 1 | -1 | -1 | 1 | -1 | 1 | 1 | 1 | -1 | -1 | 1 | 1 | 1 | 2 |
| Sum | 0 | 0 | 0 | 0 | 0 | 0 | | | | | | | | | | | | | | | | | | | |

Figure 12. Setting up the experimental design including interactions

In order to reduce the number of simulations we can reduce use a “balance” method which adds all coefficients (1 and -1 corresponding the min and max values), including all interaction terms among all 5 dimensionless terms considered, and choose only those cases for which the sum is null. In such a way we have a balance effect of all parameters among themselves. This leads us a fractional experimental design showing 8 cases. The summary of this simple method is shown in Figure 13.

| | | A | B | C | D | E | ABCDE | AB | AC | AD | AE | BC | BD | BE | CD | CE | DE | ABC | ACD | ADE | BCD | BDE | CDE | ABCD | BCDE | Sum |
|---|---|---|---|---|---|---|---|---|---|---|---|---|---|---|---|---|---|---|---|---|---|---|---|---|---|---|
| 1 | 3 | 1 | -1 | 1 | 1 | 1 | -1 | -1 | 1 | 1 | 1 | -1 | -1 | -1 | 1 | 1 | 1 | -1 | 1 | 1 | -1 | -1 | 1 | -1 | -1 | 0 |
| 2 | 8 | 1 | -1 | -1 | 1 | 1 | 1 | -1 | -1 | 1 | 1 | 1 | -1 | -1 | -1 | -1 | 1 | 1 | -1 | 1 | 1 | -1 | -1 | 1 | 1 | 0 |
| 3 | 9 | 1 | 1 | -1 | -1 | 1 | 1 | 1 | -1 | -1 | 1 | -1 | -1 | 1 | 1 | -1 | -1 | -1 | 1 | -1 | 1 | -1 | 1 | 1 | 1 | 0 |
| 4 | 10 | 1 | 1 | 1 | -1 | -1 | 1 | 1 | 1 | -1 | -1 | 1 | -1 | -1 | -1 | -1 | 1 | 1 | -1 | 1 | -1 | 1 | 1 | -1 | 1 | 0 |
| 5 | 13 | 1 | 1 | -1 | -1 | -1 | -1 | 1 | -1 | -1 | -1 | -1 | -1 | -1 | 1 | 1 | 1 | -1 | 1 | 1 | 1 | 1 | -1 | 1 | -1 | 0 |
| 6 | 18 | -1 | 1 | -1 | -1 | -1 | 1 | -1 | 1 | 1 | 1 | -1 | -1 | -1 | 1 | 1 | 1 | 1 | -1 | -1 | 1 | 1 | -1 | -1 | -1 | 0 |
| 7 | 23 | -1 | 1 | 1 | -1 | -1 | -1 | -1 | -1 | 1 | 1 | 1 | -1 | -1 | -1 | -1 | 1 | -1 | 1 | -1 | -1 | 1 | 1 | 1 | 1 | 0 |
| 8 | 24 | -1 | -1 | 1 | 1 | -1 | -1 | 1 | -1 | -1 | 1 | -1 | -1 | 1 | 1 | -1 | -1 | 1 | -1 | 1 | -1 | 1 | -1 | 1 | 1 | 0 |

Figure 13. Final experimental design covering all simulations per scenario

## 3. Simulations Set-up

In order to perform simulations one needs to define as input a geometry (grid properties), which should be refined within the storage zone. The grid shown below is common to all simulations. Below (Figure 14) we show first an X-Y view followed by a X-Z or Y-Z view of the layering chosen.

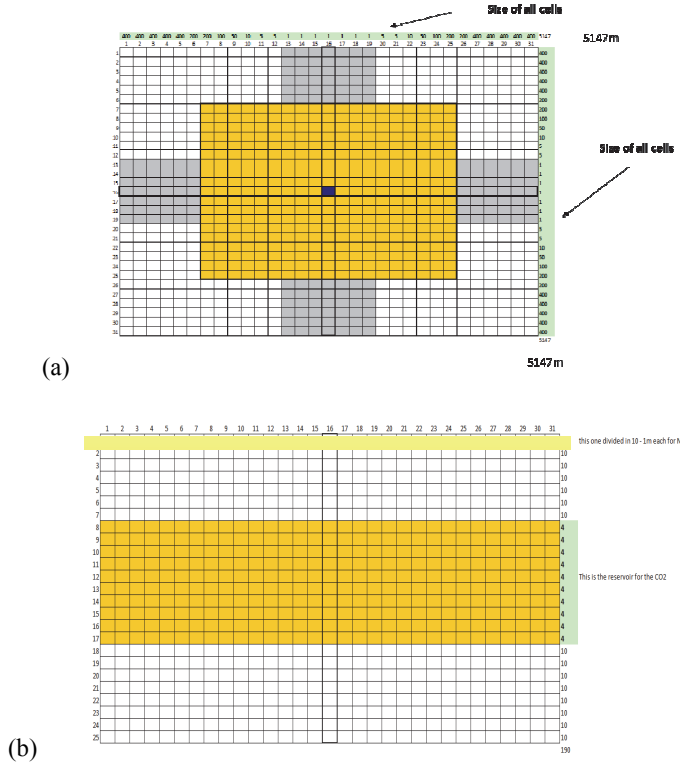
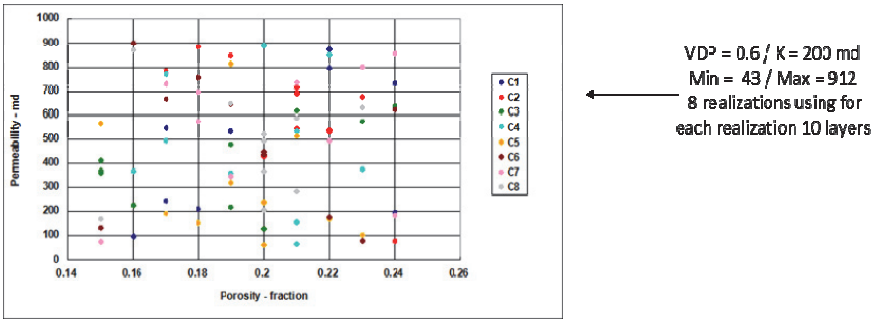



Figure 14. Grid used in X, Y and Z for all simulations: (a) X-Y and (b) X-Z or Y-Z

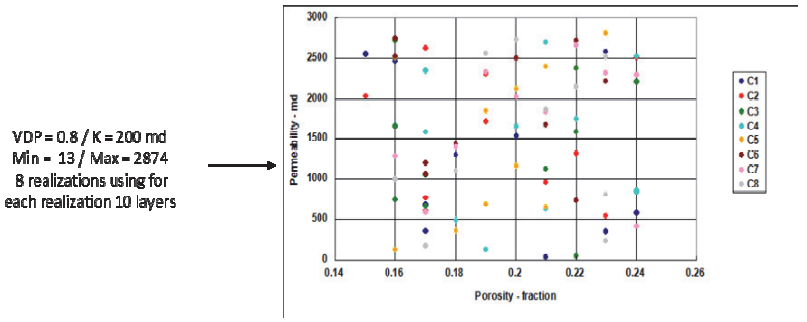
As seen the injection zone has been refined, in order to minimize gridding effects. The layer below the cap-rock is also refined, in order to catch a possible saturation evolution within the zone where the $N_2$ is supposed to be placed. The full reservoir zone is closed, considered as an injection storage zone, isolated from the rest of the field.

A petrophysical relationship between K and PHI as well as a spatial distribution of these properties has been developed using the two VDP values chosen (0.6 and 0.8), considered to cover the entire range of possible heterogeneity variation. The average permeability used is 200md and the average porosity is 0.2.

Given the VDP used the minimum permeability is 43md while the maximum is 912md for VDP = 0.6 and the minimum permeability is 13md and 2874md for VDP = 0.8. Results corresponding to a stochastic draw of 8 realizations (corresponding to the 8 cases identified as representative by the experimental design) are shown below when considering an PHI range of 0.15 to 0.24, considered as representative of reservoirs in which $CO_2$ storage will be considered (Figure 15).




(a)




(b)

Figure 15. Permeability realizations obtained for a VDP of (a) 0.6 and (b) 0.8

These values were generated at the level of the reservoir (See grid representation above) while for the rest of the simulation domain average values were used.

The actual K vs. PHI distributions are shown below. In principle the VDP concept implies an ordering of layers within the reservoir. In our case this is not the case and all values within layers are drawn randomly within the petrophysical range values indicated. The procedure consisted to first determine a unique K-PHI relationship.within a porosity range 0.15 and 0.24 (typical of potential storage aquifers). To these porosity values are associated permeability values obtained from the VDP centered around an average permeability of 200md (again typical of what storage aquifers ought to have). The final step is to draw randomly from the porosity and permeability distribution 8 realizations which establishes 8 distributions. Results are shown in Figure 16.

For VDP = 0.6

| PHI | K | PHI | K | PHI | K | PHI | K | PHI | K | PHI | K | PHI | K | PHI | K |
|---|---|---|---|---|---|---|---|---|---|---|---|---|---|---|---|
| 0.24 | 732 | 0.21 | 691 | 0.15 | 362 | 0.16 | 367 | 0.22 | 169 | 0.24 | 620 | 0.21 | 734 | 0.19 | 646 |
| 0.24 | 196 | 0.22 | 534 | 0.15 | 411 | 0.19 | 361 | 0.2 | 62 | 0.2 | 448 | 0.24 | 184 | 0.2 | 521 |
| 0.22 | 796 | 0.17 | 784 | 0.23 | 574 | 0.17 | 769 | 0.21 | 513 | 0.19 | 645 | 0.24 | 854 | 0.23 | 630 |
| 0.17 | 245 | 0.23 | 676 | 0.2 | 129 | 0.22 | 850 | 0.19 | 320 | 0.17 | 667 | 0.18 | 574 | 0.16 | 868 |
| 0.18 | 210 | 0.21 | 715 | 0.24 | 635 | 0.23 | 374 | 0.15 | 565 | 0.18 | 756 | 0.18 | 698 | 0.21 | 283 |
| 0.17 | 774 | 0.2 | 428 | 0.15 | 369 | 0.21 | 64 | 0.17 | 191 | 0.16 | 901 | 0.22 | 493 | 0.2 | 495 |
| 0.16 | 98 | 0.24 | 76 | 0.21 | 616 | 0.21 | 531 | 0.18 | 154 | 0.2 | 437 | 0.23 | 801 | 0.15 | 169 |
| 0.22 | 874 | 0.18 | 884 | 0.16 | 226 | 0.17 | 495 | 0.19 | 814 | 0.22 | 175 | 0.15 | 74 | 0.21 | 589 |
| 0.19 | 532 | 0.19 | 847 | 0.19 | 479 | 0.21 | 156 | 0.2 | 239 | 0.23 | 78 | 0.17 | 729 | 0.2 | 368 |
| 0.17 | 545 | 0.21 | 543 | 0.19 | 219 | 0.2 | 890 | 0.23 | 104 | 0.15 | 134 | 0.19 | 347 | 0.2 | 206 |

For VDP = 0.8

| PHI | K | PHI | K | PHI | K | PHI | K | PHI | K | PHI | K | PHI | K | PHI | K |
|---|---|---|---|---|---|---|---|---|---|---|---|---|---|---|---|
| 0.17 | 354 | 0.17 | 765 | 0.17 | 1054 | 0.21 | 2697 | 0.2 | 1165 | 0.16 | 2744 | 0.17 | 588 | 0.17 | 177 |
| 0.23 | 2584 | 0.23 | 536 | 0.22 | 2379 | 0.17 | 1579 | 0.19 | 685 | 0.22 | 732 | 0.22 | 2657 | 0.18 | 1103 |
| 0.2 | 1530 | 0.19 | 2312 | 0.22 | 49 | 0.24 | 2526 | 0.21 | 651 | 0.17 | 1065 | 0.18 | 1398 | 0.22 | 2150 |
| 0.15 | 2554 | 0.22 | 1317 | 0.21 | 1132 | 0.17 | 2348 | 0.23 | 2806 | 0.18 | 1435 | 0.24 | 411 | 0.16 | 998 |
| 0.18 | 1295 | 0.19 | 1725 | 0.22 | 1583 | 0.21 | 632 | 0.19 | 1855 | 0.17 | 1197 | 0.2 | 2023 | 0.19 | 2560 |
| 0.21 | 37 | 0.15 | 2036 | 0.16 | 2724 | 0.2 | 1663 | 0.16 | 127 | 0.22 | 2719 | 0.21 | 1847 | 0.21 | 1870 |
| 0.24 | 578 | 0.17 | 607 | 0.24 | 2213 | 0.24 | 852 | 0.16 | 2517 | 0.23 | 2216 | 0.23 | 2323 | 0.23 | 811 |
| 0.16 | 2466 | 0.17 | 2624 | 0.16 | 1668 | 0.22 | 1757 | 0.21 | 2396 | 0.2 | 2503 | 0.24 | 2295 | 0.2 | 2732 |
| 0.17 | 683 | 0.21 | 958 | 0.16 | 741 | 0.19 | 127 | 0.2 | 2124 | 0.16 | 2525 | 0.16 | 1285 | 0.23 | 234 |
| 0.23 | 352 | 0.24 | 2514 | 0.17 | 664 | 0.18 | 487 | 0.18 | 363 | 0.21 | 1682 | 0.19 | 2330 | 0.23 | 2519 |

Figure 16. K-PHI distributions for all simulations

A dynamic petrophysical data set (Relative permeability Kr curves for water and $CO_2$). Aside from the saturation and individual curves end-points, exponents of the curves are also needed.

The first step of this data generation is to define the maximum gas saturation trapped ($Sgt_{max}$). Since for all realizations a different porosity distribution is used, we considered the average porosity of each realization and then using the correlation of Holtz [22] we generated the corresponding trapping gas saturation. Results are show in Figure 17.

VDP = 0.6

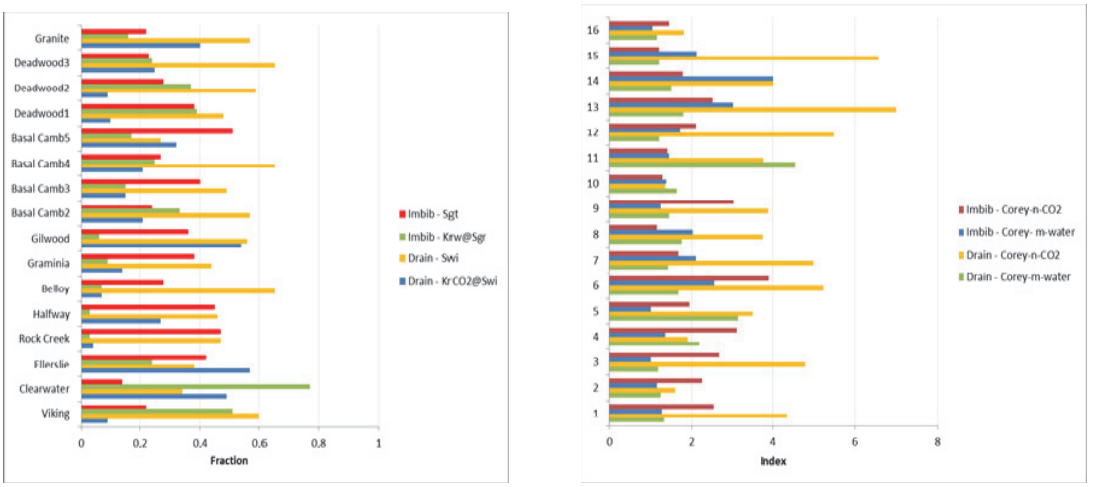
| Sim 1 | Sim2 | Sim3 | Sim4 | Sim5 | Sim6 | Sim7 | Sim8 |
|---|---|---|---|---|---|---|---|
| 0.381106893 | 0.363649342 | 0.396969158 | 0.378157216 | 0.383057333 | 0.384259012 | 0.373317673 | 0.381504725 |

VDP = 0.8

| Sim 1 | Sim2 | Sim3 | Sim4 | Sim5 | Sim6 | Sim7 | Sim8 |
|---|---|---|---|---|---|---|---|
| 0.384822981 | 0.38422881 | 0.386291817 | 0.368941326 | 0.38439346 | 0.386921737 | 0.367989639 | 0.370658978 |

Figure 17. Trapped CO2 saturation for all simulations using Holtz correlation

The second step is to generate the other end-point of the Kr curves, such as the Swi (for both imbibition and drainage curves since injection and imbibition have to be considered. The other factors concern the M and N Corey shape factors which have to be used. Since no clear data base is currently available in the literature we used values given by Bachu [8], concerning aquifers in Canada. We considered them as representative (Figure 18).




(a) (b)

Figure 18. (a) Sgt and Swi including end-points and (b) M and N Corey exponents

When summarizing all results and grouping them according to all cases simulated, for drainage and imbibition, results can be seen below (Figure 19).

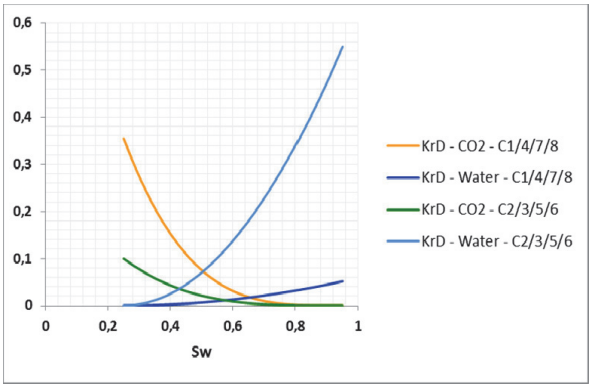



Figure 19. Kr for all cases for drainage

Given all of the above we can summarize all simulation cases along one injection scenarios corresponding to allowable overpressures varying between $1.1P_{res}$ and $1.2\ P_{res}$. These values are considered as typical low overpressures which are seen during the storage of $CH_4$ which are the only reliable historical record of storage gas overpressure in our possession. This is why we considered these values for the simulations undertaken.

In summary, what has been developed are the formulation of a few dimensionless numbers characterizing the storage, the minimum and maximum values of these from a realistic data-base of reservoirs and a few simulations based on various combinations of maximum and minimum values of these dimensionless numbers. The last step is to find common values of the parameters making up these dimensionless numbers, coherent throughout and meeting

the requirements of the min. and max. values. This step was done through an iterative, trial-and error process, leading to a data set of values which fit the best all dimensionless values.

Results are given in the next figures (Figure 20), for both injection schemes, leading to different overpressures expected during the various simulations undertaken.

| Summary | Scenario 1 (Plim from 1.1Pres to 1.23Pres) | | | | | | | |
|---|---|---|---|---|---|---|---|---|
| | 1 | 2 | 3 | 4 | 5 | 6 | 7 | 8 |
| L | 800 | 800 | 800 | 800 | 800 | 800 | 800 | 800 |
| H | 40 | 40 | 40 | 40 | 40 | 40 | 40 | 40 |
| Kx | 200 | 200 | 200 | 200 | 200 | 200 | 200 | 200 |
| Kz | 20 | 20 | 20 | 20 | 20 | 1,25 | 1,25 | 1,25 |
| alpha | 5 | 5 | 5 | 5 | 5 | 5 | 5 | 5 |
| Krw° | 0,052 | 0,55 | 0,55 | 0,052 | 0,55 | 0,55 | 0,052 | 0,052 |
| KrCO2° | 0,355 | 0,1 | 0,1 | 0,355 | 0,1 | 0,1 | 0,355 | 0,355 |
| Muw | 0,8 | 0,8 | 0,8 | 0,8 | 0,8 | 0,8 | 0,8 | 0,8 |
| MuCO2 | 0,1 | 0,1 | 0,1 | 0,1 | 0,1 | 0,1 | 0,1 | 0,1 |
| rhow | 1200 | 1200 | 1200 | 1200 | 1200 | 1200 | 1200 | 1200 |
| rhoCO2 | 500 | 500 | 500 | 500 | 500 | 500 | 500 | 500 |
| Pres | 14000 | 14000 | 14000 | 14000 | 14000 | 14000 | 14000 | 14000 |
| Pinj | 15400 | 15400 | 15400 | 25200 | 25200 | 25200 | 25200 | 15400 |
| PHI | 0,25 | 0,25 | 0,25 | 0,25 | 0,25 | 0,25 | 0,25 | 0,25 |
| sigma | 40 | 40 | 40 | 40 | 40 | 40 | 40 | 40 |

Figure 20. All cases for the injection scenarios Pinj = 1.1/1.2Pres

An initial temperature and pressure: the initial temperature was set at 54°C (ad-hoc) whereas the initial pressure is taken as 140bars, in the middle of the perforated interval.

An injection rate corresponding to the $CO_2$ placement stage - injection stage: the injection rate chosen is 1M tons $CO_2$/year. This value is often used as a "standard" in $CO_2$ injection scenarios. The injection is supposed to occur over the entire reservoir height. The reservoir height considered are supposed to be realistic. Injection is set to occur for 4 years. This is followed by a resting period set to 10 years during which time the saturation is slowly equilibrates as the pressure diffuses throughout the reservoir.

The total number of simulations is 16 corresponding to the injection scenario, for the two heterogeneity factors used. Throughout the full simulation the $CO_2$ saturation is monitored so as not to contaminate the layer below the cap-rock (refined into 10 thin layers) where the $N_2$ is supposed to be injected as a protective, cushion measure.

## 4. RESULTS and DISCUSSION

Among all results (16 cases simulated) only 5 are recognized as being favorable for an eventual $N_2$ injection as a preventive leaking measure, since no $CO_2$ reached the upper layer, neither at the end of the injection period, nor after the resting period of 10 years. The favorable cases were Case 6/7/14/15 and 16. These cases show the following dimensionless numbers (see Figure 21)

| Case | Aspect Ratio | Dip | Mobility Ratio | Buoyancy Nb. | Capillary Nb. | Sgr | VDP |
|---|---|---|---|---|---|---|---|
| 6 | 1.58 | 3.52 | 1.45 | 13.89 | 0.000301 | 0.38 | 0.6 |
| 7 | 1.58 | 3.52 | 54.61 | 13.89 | 0.000301 | 0.37 | 0.6 |
| 14 | 1.58 | 3.52 | 1.45 | 13.89 | 0.000301 | 0.38 | 0.8 |
| 15 | 1.58 | 3.52 | 54.61 | 13.89 | 0.000301 | 0.37 | 0.8 |
| 16 | 1.58 | 0.17 | 54.61 | 1562.1 | 0.000301 | 0.38 | 0.8 |

Figure 21. Dimensionless numbers for all favorable N2 cases

The first remark when inspecting these results is the fact that two have a VDP of 0.6 (more homogeneous) while three cases have a VDP of 0.8 (more heterogeneous). Thus, heterogeneity doesn't play an important role in the $CO_2$ placement with regard to the cap-rock. All favorable cases have the same aspect ratio (low), the same capillary number, almost the same Sgr and the same buoyancy number, Ng (low). The role of the vertical movement due to low Ng and low vertical permeability Kz, which enters in the aspect ratio term is evident. Those two numbers drive the $CO_2$ setting, and therefore the capacity of the $CO_2$ to eventually contaminate the upper layer where the $N_2$ would be injected. The role of the mobility ratio is more ambiguous and plays a role when the gravity number is high (Case16). Let's look at the regulating role of the mobility ratio by comparing Cases 6 and 7.

For case 6 (considered as a typical favorable case) the situation at the end of the injection period (4years) shows a favorable $CO_2$ saturation, which has not reached the upper layer. When looking at the evolution of the saturation during the resting period, the $CO_2$ remains within the original region of storage, moving only slightly. The lateral movement, governed by the mobility number, compensates the vertical movement adequately. This is shown in Figure 22.

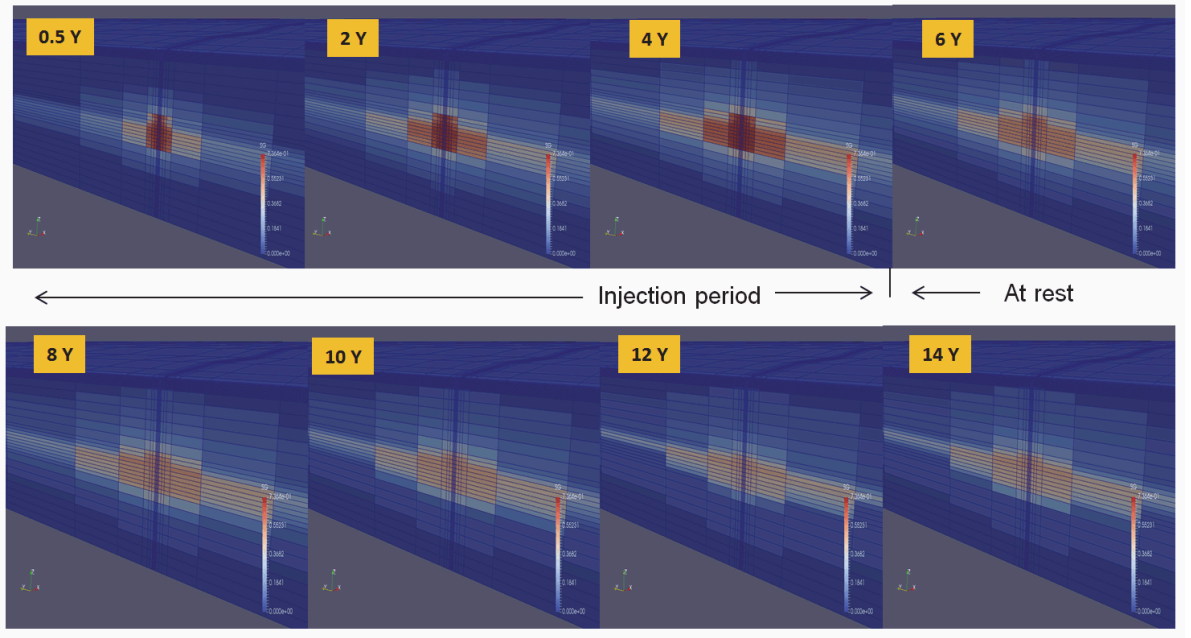



Figure 22. Case 6 - $CO_2$ saturation evolution

When looking at Case 7, for which the Mobility number is higher, the general saturation shows a propensity to spread more, given the K-PHI distribution (comparison of the $CO_2$ saturation zone between Case 6 and 7) which are certainly different yet both having variance values corresponding to a common VDP (0.6), thus statistically equivalent.

For both cases the maximum $CO_2$ saturation obtained at the end of 4 years of injection is almost identical, namely 0.7364 and 0.7267. Therefore, comparing the spread between these two cases can become significant. The situation can be seen in Figure 23.

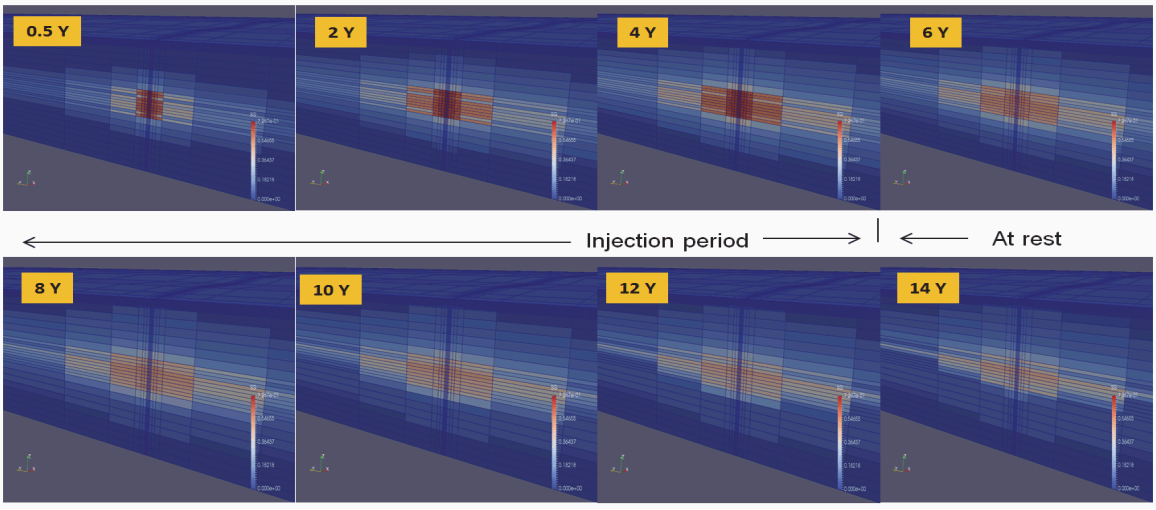



Figure 23. Case 7 saturation evolution

By opposition, if we look at an unfavorable case (Case9) the aspect ratio is 6.32 (max) instead of 1.38 (min) implying that the favorable vertical permeability favors the vertical movement. This can be seen in Figure 24.

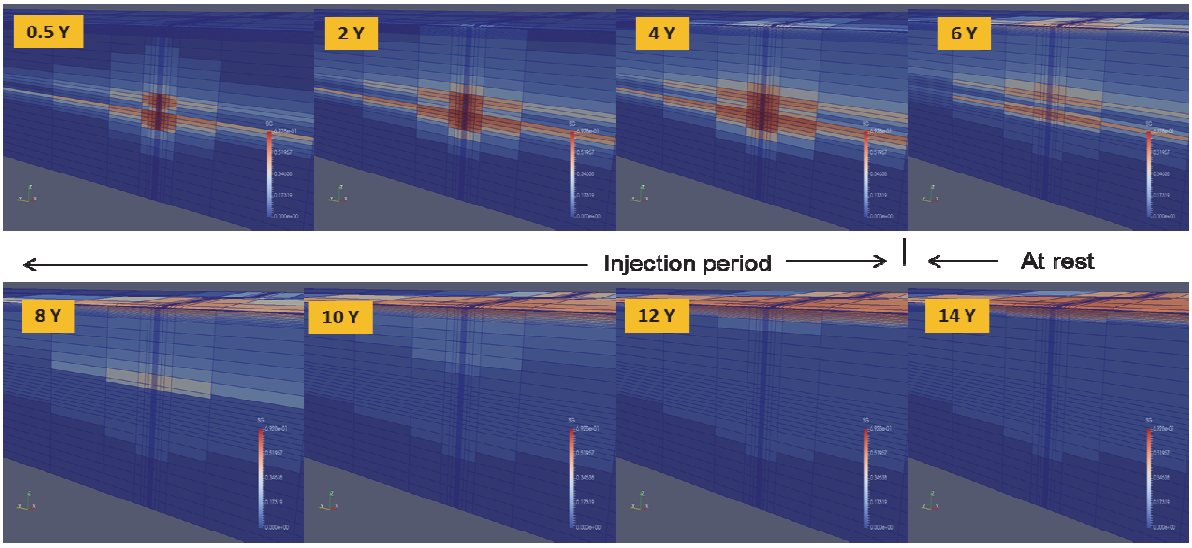



Figure 24. Case 9 - $CO_2$ saturation evolution ( unfavorable)

The same situation occurs for all the other cases. For example the maximum saturations reached for Cases 14, 15 and 16 are respectively 0.688, 0.672 and 0.677. A different situation occurs for Case 16 which shows, when looking at the dimensionless numbers, a high Gravity number and a high Mobility number. This is the only case for which the saturation distribution is still favorable for the $CO_2$ saturation (Figure 25).

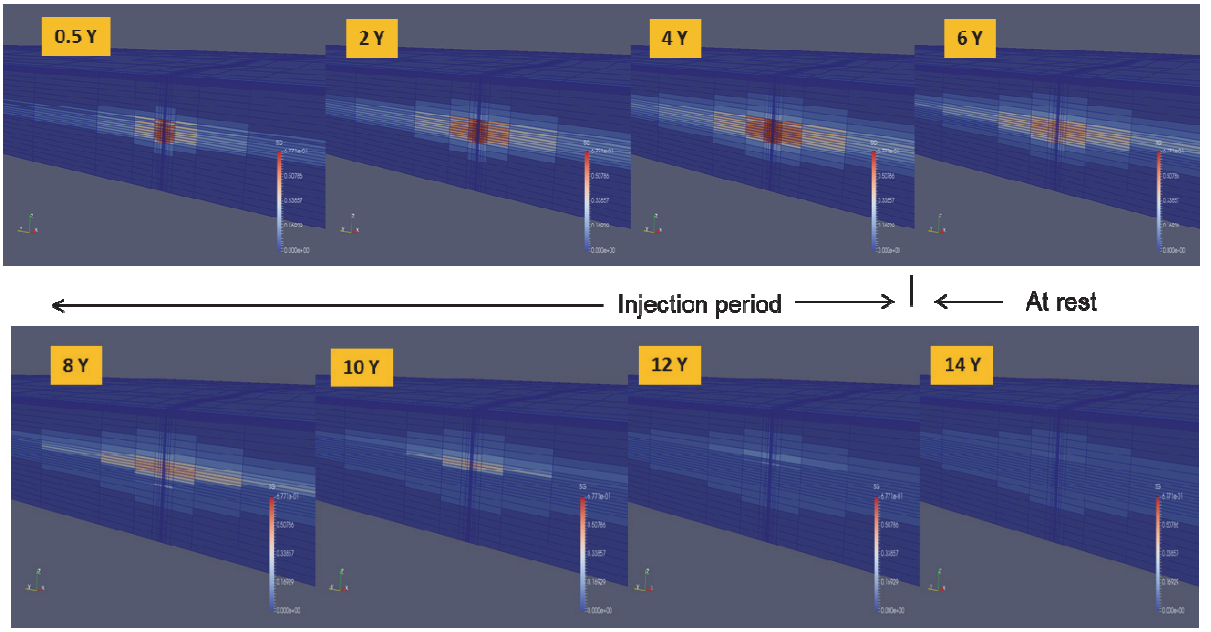



Figure 25. Case 16 - $CO_2$ saturation evolution

The situation is similar to Case 9, shown above. Yet, the difference is that for this particular case, a low Aspect Ratio is present (1.58) which proves that the Aspect Ratio is very important. In conclusion we can state that a low Aspect Ratio, high Mobility and low Gravity number are important parameters to estimate, prior to the possible injection of $N_2$.

## 5. CONCLUSIONS

- A realistic set of dimensionless numbers, characterizing the storage of $CO_2$ has been developed.
- Based on these dimensionless numbers, a data-base of values from different projects currently operating, or to be operated has been developed. Using minimum and maximum values of these numbers, a full experimental design, followed by a simplification, led to a minimal set of simulations studying the movement of the $CO_2$ in relation to a potential storage layer containing $N_2$.
- $N_2$ is conceptually imagined as a potential shield agent against $CO_2$ leaking, while potentially increasing the storage capacity of a site.
- The study of the $CO_2$ saturation distribution throughout the reservoir in regard to a potential layer containing the shielding $N_2$, has identified three main factors keeping the $CO_2$ in place. These are the Aspect Ratio, the Buoyancy number (Gravity Number) and the Mobility Ratio. While the first two govern the vertical movement of the $CO_2$, the last one controls the lateral extension of the $CO_2$. For these numbers, a low aspect ratio, combined

with low Gravity number and a High Mobility number insures that $CO_2$ stays within the reservoir throughout the injection period.

- It is clear that the cases studied correspond to a specific injection rate, distance between the reservoir and the $N_2$ storage layer, and a specific period time of injection. A more refined study is needed to determine the relationship between injection rate, distance between reservoir and $N_2$ and time of injection. Within the range of values chosen, out conclusions are valid for the design of a $N_2$ placement prior to the injection of $CO_2$.

## REFERENCES


[1] Shook, M. Lake, L.M. and Li, D.: "Scaling Immiscible Flow Through Permeable Media by Inspectional Analysis" In Situ, 16(4), 311-349, 1992

[2] Rivas, O., Embid, S. and Bolivar, F.: "Ranking Reservoirs for $CO_2$ Flooding Processes", SPE 23641 presented at the 1992 SPE Latin American Petroleum Engineering Conference, Caracas, March 8-11

[3] Diaz, D., Bassiouni, Z., Kimbrell, W., and Wolcott, J. : "Screening Criteria for Application of Carbon Dioxide Miscible Displacement in Waterflooded Reservoirs Containing Light Oil", SPE 35431 presented at the 1996 SPE Improved Oil recovery Symposium, Tulsa, April 21-24

[4] Hirasaki, G., Steward W.C., Elkins, L.E., Wilhite, P.G. "Reply to Discussion of the National Petroleum Council Study on EOR", SPE 20007, Journal of Petroleum Technology, Nov. 1989

[5] Jensen JL, Lake LW, Corbett P, Goggin D. Statistics for petroleum engineers and geoscientists: Handbook of petroleum exploration and production 2 (HPEP). Elsevier, 2000.

[6] Dykstra, H, and R,L, Parsons: "The Prediction of Oil Recovery by Water Flood," Secondary Recovery of Oil in the United States, Principles and Practice, 2nd ed, Amer, Pet. Inst, (1950), 160-17 4.

[7] Bachu, S., Nordbotten, J.M., Celia, M.A. "Evaluation of the spread of acid gas plumes injected in deep saline aquifers in western Canada as an analogue for CO2 injection in continental sedimentary basins" GHGT-7 Paper ID Nb.12 revised

[8] Bachu, S., 2013. Drainage and imbibition CO2/brine relative permeability curves at in situ conditions for sandstone formations in Western Canada. Energy Proc. – 11th Int. Conf. Greenhouse. Gas Control Technol. 37, 4428–4436.

[9] Flett, M., Taggart, I., Lewis J., and Gurdon, R. "Subsurface sensitivity Study of Geologic $CO_2$ Sequestration in Saline Formations" 2nd Annual Conf. on Carbon Sequestration, Alexandria, VA May 5-8, 2003.

[10] Hosa, A., Esentia, M., Stewart, J., Haszeldine S., "Benchmarking worldwide $CO_2$ saline aquifer injections" Scottish Center for Carbon Capture and Storage, March 2010

[11] Salathiel, R., 1973. Oil recovery by surface film drainage in mixed-wettability rocks. J. Petrol. Technol. 25, 1216–1224.

[12] Taber, J., 1969. Dynamic and static forces required to remove a discontinuous oil phase from porous media containing both oil and water. SPE J. 9, 3–12.

[13] Lake, L., Johns, R., Rossen, B., Pope, G., 2014. Fundamentals of Enhanced Oil Recovery. Society of Petroleum Engineers, TX, USA.

[14] Broseta, D., Tonnet, N., Shah, V., 2012. Are rocks still water-wet in the presence of dense $CO_2$ or $H_2S$? Geofluids 12, 280–294.

[15] Chiquet, P., Broseta, D., Thibeau, S., 2007. Wettability alteration of caprock minerals by carbon dioxide. Geofluids 7, 112–122

[16] Iglauer, S., Pentland, C., Bush, A., 2014a. $CO_2$ wettability of seal and reservoir rocks and the implications for carbon geosequestration. Water Resour. Res.

[17] Espinoza, D.N., Santamarina, J.C., 2010. Water-$CO_2$-mineral systems: Interfacial tension, contact angle, and diffusion–implications to $CO_2$ geological storage. Water Resour. Res. 46, W07537

[18] Farokhpoor, R., Bjorkvik, B., Lindeberg, E., Torsaeter, O., 2013. Wettability behaviour of $CO_2$ at storage conditions. Int. J. Greenh. Gas Control 12, 18–25.

[19] Wang, F., 1988. Effect of wettability alteration on water/oil relative permeability, dispersion, and flowable saturation in porous media. SPE Reserv. Eng. 3, 617–628.

[20] Saraji, S., Goual, L., Piri, M., Plancher, H., 2013. Wettability of supercritical carbon dioxide/water/quartz systems: Simultaneous measurement of contact angle and interfacial tension at reservoir conditions. Langmuir 29, 6856–6866.

[21] Iglauer, S., Salamah, A., Sarmadivaleh, M., Liu, K., Phan, C., 2014b. Contamination of silica surfaces: Impact on water-$CO_2$-quartz and glass contact angle measurements. Int. J. Greenh. Gas Control 22, 325–328.

[22] Holtz, M.H., "Residual Gas Saturation to Aquifer Influx: A Calculation Method for 3-D Computer Reservoir Model Construction", SPE 75502, SPE Gas Technology Symposium held in Calgary, Alberta, Canada, 30 April–2 May 2002.

[23] Hadlow, R.E. "Update of Industry Experience with $CO_2$ Injection" SPE 24928, 67th ATCE held in Washington, DC, October 4-7, 1992

[24]Barroux C. Method for maintaining a gas volume in an underground geological reservoir by nitrogen injection - EP 2565371 A1

[25] Fischer S., Szizybalski A., Zimmer M., Kujawa C., Plessen B., Liebscher A., Moeller F. "$N_2$-$CO_2$ co-injection field test at the Ketzin pilot CO2 storage site" Energy Procedia 63 (2014) 2848 – 2854

[26] Wei N., Li X., Wang Y., Wang Y., Kong W. "Numerical study on the field-scale aquifer storage of $CO_2$ containing $N_2$" Energy Procedia 37 (2013) 3952 – 3959